

Efficient Implementation of a van der Waals Density Functional: Application to Double-Wall Carbon Nanotubes

Guillermo Román-Pérez and José M. Soler

Departamento de Física de la Materia Condensada, C-III, Universidad Autónoma de Madrid, E-28049 Madrid, Spain

(Received 1 December 2008; published 27 August 2009)

We present an efficient implementation of the van der Waals density functional of Dion *et al.* [Phys. Rev. Lett. **92**, 246401 (2004)], which expresses the nonlocal correlation energy as a double spatial integral. We factorize the integration kernel and use fast Fourier transforms to evaluate the self-consistent potential, total energy, and atomic forces, in $O(N \log N)$ operations. The resulting overhead, for medium and large systems, is a small fraction of the total computational cost, representing a dramatic speedup over the $O(N^2)$ evaluation of the double integral. This opens the realm of first-principles simulations to the large systems of interest in soft matter and biomolecular problems. We apply the method to calculate the binding energies and the barriers for relative translation and rotation in double-wall carbon nanotubes.

DOI: 10.1103/PhysRevLett.103.096102

PACS numbers: 61.46.Fg, 31.15.eg, 71.15.-m

Density functional theory (DFT) has become the method of choice for first-principles simulations of static and dynamical properties of complex materials with strong ionic, covalent, and metallic interactions. However, weak van der Waals (vdW) interactions are also essential for many systems and processes, like molecular solids and liquids, surface adsorption, and biological reactions [1]. Local or semilocal density functionals obviously cannot describe asymptotically the nonlocal dispersion correlations. At binding distances, they have been frequently found to give reasonable results in some cases [2,3] but their ability to do so is generally very sensitive to the specific functional used and its parametrization details, making this approach rather questionable and unreliable. Thus, the simulation of vdW systems has typically relied on atom-atom potentials with the conventional [4] r^{-6} asymptotic behavior and with parameters fitted to empirical data or to accurate quantum chemistry calculations of simple molecules. Such potentials are also added as plug-ins to *ab initio* semilocal density functionals [5,6]. Another approach includes vdW interactions through effective atom-electron pseudopotentials [7]. However, the accuracy and reliability of such approaches is limited because vdW energies arise from electron-electron correlations that depend not only on the atomic species but also on their chemical environment. More *ab initio* wave function-dependent approaches are more reliable but also much more expensive [8].

Thus, a key development has been the proposal by Dion *et al.* [9] of a universal nonlocal energy functional of the electron density $n(\mathbf{r})$ with the form

$$E_{xc}[n(\mathbf{r})] = E_x^{\text{GGA}}[n(\mathbf{r})] + E_c^{\text{LDA}}[n(\mathbf{r})] + E_c^{\text{nl}}[n(\mathbf{r})] \quad (1)$$

where the exchange energy E_x^{GGA} is described through the semilocal generalized gradient approximation (GGA) [10] and the correlation energy has a local part E_c^{LDA} , described in the local density approximation (LDA), and a nonlocal (nl) part E_c^{nl} given by

$$E_c^{\text{nl}}[n(\mathbf{r})] = \frac{1}{2} \iint d^3\mathbf{r}_1 d^3\mathbf{r}_2 n(\mathbf{r}_1) n(\mathbf{r}_2) \phi(q_1, q_2, r_{12}) \quad (2)$$

where $r_{12} = |\mathbf{r}_1 - \mathbf{r}_2|$, and q_1, q_2 are the values of a universal function $q_0[n(\mathbf{r}), |\nabla n(\mathbf{r})|]$, evaluated at \mathbf{r}_1 and \mathbf{r}_2 . The kernel ϕ has also a precise and universal form that in fact depends only on two variables $d_1 = q_1 r_{12}$ and $d_2 = q_2 r_{12}$, but it can obviously be written also as a function of q_1, q_2 , and r_{12} , what we will find convenient. The shape of ϕ obeys that: (i) E_c^{nl} is strictly zero for any system with constant density; and (ii) the interaction between any two molecules has the correct r^{-6} dependence for large separations r . Using a direct evaluation of Eq. (2), this vdW functional has been applied successfully to a variety of systems, including interactions between pairs of atoms and molecules, molecules adsorbed on surfaces, molecular solids, and biological systems [11]. However, the double spatial integral poses prohibitive computational demands for the very large scale simulations required in soft-matter and biomolecular problems. For such systems, a new algorithm is needed to improve the efficiency and the scaling with system size.

If q_1 and q_2 in Eq. (2) were fixed values, independent of \mathbf{r}_1 and \mathbf{r}_2 , E_c^{nl} would be a simple convolution, like the Coulomb energy, that could be evaluated by Fourier methods. Therefore, our key step for an efficient implementation is to expand the kernel ϕ as

$$\phi(q_1, q_2, r_{12}) \simeq \sum_{\alpha\beta} \phi(q_\alpha, q_\beta, r_{12}) p_\alpha(q_1) p_\beta(q_2) \quad (3)$$

where q_α are *fixed* values, chosen to ensure a good interpolation of function ϕ . In order to illustrate how the factorization (3) can be performed in a systematic way, we consider first the interpolation of a function $f(x)$ using a linear scheme, like those of Lagrange, Fourier, or splines: $f(x) \simeq \sum_\alpha f_\alpha p_\alpha(x)$, where $f_\alpha = f(x_\alpha)$ and $p_\alpha(x)$ is the function resulting from the interpolation of the particular values $f_\beta = \delta_{\alpha\beta}$. In Lagrange interpolation, it is a poly-

nomial of given order. In Fourier interpolation it has the form $\sin[\pi(x - x_\alpha)/\Delta x]/[\pi(x - x_\alpha)/\Delta x]$. We use cubic splines, in which $p_\alpha(x)$ is a succession of cubic polynomials in every interval $[x_\beta, x_{\beta+1}]$, matching in value and the first two derivatives at every point x_β . Notice that $p_\alpha(x)$ depends on the interpolation scheme and on the (fixed) points x_α , but not on the interpolated function. In two-dimensional interpolation, one typically interpolates first in one variable and then in the other:

$$f(x, y) \approx \sum_\beta f(x, y_\beta) p_\beta(y) \approx \sum_\beta \left(\sum_\alpha f(x_\alpha, y_\beta) p_\alpha(x) \right) p_\beta(y) \quad (4)$$

which shows that such an interpolation leads automatically to an expansion in terms of factored functions of x and y . Thus, Eq. (3) is just the interpolation of a three-dimensional function in its first two variables. In this latter case, however, the interpolation points q_α must be appropriate for every value of the third variable r_{12} .

The fact that r_{12} acts as a scaling factor (i.e., increasing r_{12} merely “contracts” ϕ as a function of q_1 and q_2 , without changing its shape) suggests a logarithmic mesh of points q_α , in which $(q_{\alpha+1} - q_\alpha) = \lambda(q_\alpha - q_{\alpha-1})$, with $\lambda > 1$. Such a logarithmic mesh is also suggested by the shape of $\phi(d_1, d_2)$ shown in Fig. 1 of Ref. [9]. We have found that $N_\alpha \sim 20$ interpolation points q_α are sufficient for an accurate description of ϕ up to a cutoff q_c at which we artificially “saturate” the original function $q_0(n, |\nabla n|)$ by redefining $q_0^{\text{sat}}(n, |\nabla n|) = h[q_0(n, |\nabla n|), q_c]$, where $h(x, x_c)$ is a smooth function such that $h(x, x_c) \approx x$ for $x < x_c$ and $h(x, x_c) \rightarrow x_c$ for $x \rightarrow \infty$:

$$h(x, x_c) = x_c \left[1 - \exp\left(-\sum_{m=1}^{m_c} \frac{(x/x_c)^m}{m}\right) \right] \quad (5)$$

with $m_c \sim 12$ and $q_c \sim 5$ a.u.. Higher q_0 values are obtained only for very large $n(\mathbf{r})$ (i.e., close to the nucleus, where E_c^{nl} is negligible compared to other terms in E_{xc}), and for large $|\nabla n|/n$ [in the electron density tails, where E_c^{nl} is negligible because of the factor $n(\mathbf{r})$ in the integrand of Eq. (2)]. In what follows, we will omit, but assume, super index “sat” in $q_0(n, |\nabla n|)$.

A minor but significant difficulty is that $\phi(d_1, d_2)$ has a logarithmic divergence when $d_1, d_2 \rightarrow 0$, what prevents its straightforward interpolation. Therefore, we interpolate and use instead a modified “soft” form

$$\phi_s(d_1, d_2) = \begin{cases} \phi_0 + \phi_2 d^2 + \phi_4 d^4 & \text{if } d < d_s \\ \phi(d_1, d_2) & \text{otherwise,} \end{cases} \quad (6)$$

where $d = \sqrt{d_1^2 + d_2^2}$. ϕ_0 and d_s are fixed parameters, and ϕ_2, ϕ_4 are adjusted so that $\phi_s(d_1, d_2)$ and $\phi(d_1, d_2)$ match in value and slope at $d = d_s$ (for given d_2/d_1). This modification leads to a change in E_c^{nl} , which is corrected using a local density approximation, $\Delta E_c^{\text{nl}} = \int d^3 \mathbf{r} n(\mathbf{r}) \Delta \epsilon_c^{\text{nl}}(\mathbf{r})$, where

$$\Delta \epsilon_c^{\text{nl}}(\mathbf{r}) = \frac{n(\mathbf{r})}{2} \int_0^\infty 4\pi r'^2 dr' [\phi(q, q, r') - \phi_s(q, q, r')] \quad (7)$$

with $q = q_0(n(\mathbf{r}), \nabla n(\mathbf{r}))$. The evaluation of ΔE_c^{nl} and its derivatives is performed, like that of the semilocal terms in Eq. (1), as in Ref. [12]. In what follows, we will assume, but omit for simplicity, the subindex s in ϕ_s .

Substitution of (3) into (2) leads to

$$\begin{aligned} E_c^{\text{nl}} &= \frac{1}{2} \sum_{\alpha\beta} \iint d^3 \mathbf{r}_1 d^3 \mathbf{r}_2 \theta_\alpha(\mathbf{r}_1) \theta_\beta(\mathbf{r}_2) \phi_{\alpha\beta}(r_{12}) \\ &= \frac{1}{2} \sum_{\alpha\beta} \int d^3 \mathbf{k} \theta_\alpha^*(\mathbf{k}) \theta_\beta(\mathbf{k}) \phi_{\alpha\beta}(k) \end{aligned} \quad (8)$$

where $\theta_\alpha(\mathbf{r}) = n(\mathbf{r}) p_\alpha[q_0(n(\mathbf{r}), \nabla n(\mathbf{r}))]$ and $\theta_\alpha(\mathbf{k})$ is its Fourier transform. Equally, $\phi_{\alpha\beta}(k)$ is the Fourier transform of $\phi_{\alpha\beta}(r) \equiv \phi(q_\alpha, q_\beta, r)$. It can be calculated in spherical coordinates, and stored in a radial mesh of points k for convenient interpolation. Thus, the heavier part of the calculation is the fast Fourier transforms of the N_α functions $\theta_\alpha(\mathbf{r})$, which still have a very moderate cost in a typical density functional calculation.

The evaluation of atomic forces requires the use of the Hellman-Feynman theorem, which holds only if the full energy functional is minimized self-consistently. In turn, this requires the nonlocal part of the correlation potential, i.e., the functional derivative of Eq. (2) [13]. To handle the gradient dependence in $q_0(n, \nabla n)$ we use the same technique as in Ref. [12]: approximating the spatial integrals by sums in a uniform grid of points, and the gradients by finite differences in the same grid. This makes E_c^{nl} an ordinary function of the densities n_i at fixed grid points \mathbf{r}_i , allowing us to perform conventional partial derivatives, rather than functional derivatives. Besides its conceptual simplicity, this method ensures a perfect consistency between the calculated potential and the energy:

$$E_c^{\text{nl}} = \frac{1}{2} \Delta \Omega^2 \sum_{\alpha\beta} \sum_{ij} \theta_{\alpha i} \theta_{\beta j} \phi_{\alpha\beta}(r_{ij}), \quad (9)$$

where $\Delta \Omega$ is the volume per grid point and $\theta_{\alpha i} \equiv n_i p_\alpha[q_0(n_i, \nabla n_i)]$. Notice that $\phi_{\alpha\beta}(r_{ij})$ does not depend on n_i , since the values q_α are fixed. Thus, defining $v_i^{\text{nl}} \equiv (\partial E_c^{\text{nl}} / \partial n_i) / \Delta \Omega$, we obtain

$$v_i^{\text{nl}} = \sum_\alpha \left(u_{\alpha i} \frac{\partial \theta_{\alpha i}}{\partial n_i} + \sum_j u_{\alpha j} \frac{\partial \theta_{\alpha j}}{\partial \nabla n_j} \frac{\partial \nabla n_j}{\partial n_i} \right), \quad (10)$$

where $\partial \nabla n_j / \partial n_i$ are fixed coefficients (determined by the finite difference formula used for ∇n_j) that depend only on \mathbf{r}_{ij} and that are nonzero only for small r_{ij} . Also,

$$u_{\alpha i} = \Delta \Omega \sum_\beta \sum_j \theta_{\beta j} \phi_{\alpha\beta}(r_{ij}) \quad (11)$$

is a convolution that can be obtained using fast Fourier transforms since (apart from π and volume factors)

$$\int d^3 \mathbf{r}_2 \theta_\beta(\mathbf{r}_2) \phi_{\alpha\beta}(r_{12}) = \int d^3 \mathbf{k} e^{i\mathbf{k}\mathbf{r}_1} \theta_\beta(\mathbf{k}) \phi_{\alpha\beta}(k). \quad (12)$$

Thus, a self-consistency step requires N_α direct transforms to find $\theta_\alpha(\mathbf{k})$ and N_α inverse transforms to obtain $u_\alpha(\mathbf{r})$. The calculation of the atomic forces does not require any additional effort, since the nonlocal contribution v_i^{nl} is simply added to the semilocal terms [12] in v_i^{xc} and to the rest of the effective potential. Notice that the implementation is independent of the basis set, accepting $n(\mathbf{r}_i)$ in a uniform real-space grid \mathbf{r}_i and returning E_{xc} and $v_{\text{xc}}(\mathbf{r}_i)$ in the same grid. It has been checked [14] that it reproduces accurately the results obtained by direct evaluation of Eq. (2) and its functional derivative [13], and it has been already used to study hydrogen adsorption in a large metal organic framework [15].

Kleis *et al.* [16] have studied previously the interaction between parallel, nonconcentric carbon nanotubes, using the vdW density functional. We have applied our implementation to study the interaction between the concentric layers of double-wall carbon nanotubes (DWNTs). Such interactions are crucial for different nanodevices proposed recently [17,18] and they have been studied with semi-empirical potentials [19] and with a local DFT functional [20–22]. We have used the SIESTA code [23,24] with an optimized [25] triple- ζ + polarization basis set of pseudo atomic orbitals, correcting for basis set superposition errors (BSSE). The integration grids in real and reciprocal space had cutoffs of 300 Ry and 20 Å [26] respectively, ensuring at least 34, 20, and 14 k points for the armchair, zigzag, and chiral DWNTs studied. The atomic forces were relaxed to less than 20 meV/Å.

Figure 1 shows the calculated interaction energy between two rigid single-wall nanotubes (SWNTs) (relaxed independently) as a function of their interwall separation (difference of radii). It also shows the DWNT formation energies, defined as the difference between the total energy of the relaxed DWNT and that of the two SWNTs. The calculated tubes $(m, m)@(n, n)$ (armchair), $(m, 0)@(n, 0)$ (zigzag) and $(8, 2)@(16, 4)$ (chiral) were chosen for their commensurability in the longitudinal direction, as well as for comparison with prior calculations. Several conclusions can be reached from the figure: (i) The LDA underestimates the interaction by a factor of 2. (ii) The interaction energy per atom depends negligibly on the nanotube chirality and size (curvature), being very well represented by the interaction between two flat graphene layers. (iii) The relaxation of the radii, induced by the interaction, leads to a steeper repulsion than between flat graphene layers. (iv) For sufficiently long tubes, in which the border effects can be neglected, the calculated vdW interaction energy gives a telescopic contraction force [18] $F = 0.29 \text{ N/m} \times C$, where C is the mean of the inner and outer tube circumference lengths. This is in reasonable agreement with the experimental value of 0.16 N/m [27], given the experimental uncertainties.

We also calculated the spatial distribution of the non-local energy density, i.e., of the integrand of Eq. (2) integrated over one of the two positions [28]. It can be seen

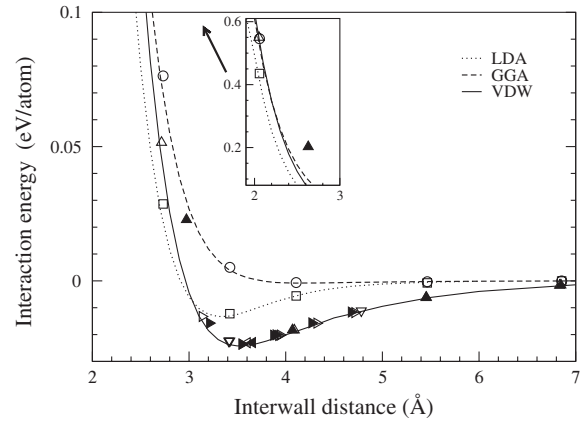


FIG. 1. Interaction and formation energies between different double-wall carbon nanotubes, as a function of interwall separation, using LDA [29] (squares), GGA [30] (circles), and van der Waals [9] (triangles) functionals. Interaction energies (empty symbols) are between two individually relaxed rigid tubes. Formation energies (filled symbols) include also the geometry relaxation induced by the interaction, that modifies their interwall separation. The tube geometries are $(5, 5)@(n, n)$ ($\square, \square, \triangle$), $(m, m)@(n, n)$ $m > 5$ (∇), $(m, 0)@(n, 0)$ (\triangleright), and $(8, 2)@(16, 4)$ (\triangleleft). For comparison, we also show the interaction energies for two flat graphene layers (lines). All energies are divided by the total number of atoms in both tubes. Our estimated error bar is ~ 1 meV/atom.

that such energy densities are concentrated in the outer side of the inner tube and in the inner side of the outer tube, but otherwise following closely the electron density distributions.

Next, the two concentric tubes of the DWNTs were moved rigidly, relative to each other, in order to construct rotation-translation energy maps. To represent the calculated maps, we first project the inner tube coordinates onto the outer tube surface, i.e., we multiply its x and y coordinates (the tube axis being z) by the ratio $R_{\text{out}}/R_{\text{in}}$ between the two radii. We then unroll the coordinates of both tubes onto a flat surface, repeating them periodically also in the x axis. This gives two flat periodic lattices (commensurate in the cases considered) with reciprocal unit cell vectors \mathbf{a}_i and \mathbf{b}_i , $i = 1, 2$. The energy maps can then be represented, as a function of the position \mathbf{x} on this surface, relative to the minimum, by an expansion of the form

$$U(\mathbf{x}) = U_0 - \frac{1}{4} \sum_{\mathbf{G} \neq 0} U_{\mathbf{G}} \cos(\mathbf{G} \cdot \mathbf{x}) \quad (13)$$

where \mathbf{G} are the super lattice wave vectors, common to the reciprocal lattices \mathbf{a} and \mathbf{b} , and $U_{\mathbf{G}}$ are the barrier heights for motion along \mathbf{G} . We have found that limiting this expansion to the first two wave vector stars, $\pm \mathbf{G}_1$ and $\pm \mathbf{G}_2$ (which, in the cases studied, are parallel and orthogonal to the axial direction), gives a good approximation to the cases studied, with the parameters given in Table I.

Overall, the relative values of these barrier heights are in qualitative agreement with previous calculations, i.e.,

TABLE I. Periodicities ($\Delta x_i = 2\pi/G_i$, in Å) and energy barriers U_i (in meV per outer tube atom) for translation ($i = z$) and rotation ($i = \phi$) of the outer tube, relative to the inner tube, in double-wall carbon nanotubes. Δx_ϕ lengths are along the outer tube circumference. For the (8, 2)@(16, 4) tube we found that all the LDA and vdW barriers are smaller than our computational accuracy of ~ 0.01 meV/atom.

DWNT	(5, 5)@(10, 10)	(9, 0)@(18, 0)	(8, 2)@(16, 4)
Δx_z	1.24	2.15	0.47
Δx_ϕ	2.15	1.24	0.81
U_z^{LDA}	0.07	1.38	0.00
U_ϕ^{LDA}	0.48	0.16	0.00
U_z^{vdW}	0.04	1.22	0.00
U_ϕ^{vdW}	0.43	0.06	0.00

larger barrier distances lead to larger barrier heights. Quantitatively, however, those calculations vary by an order of magnitude depending on the models used [19,20]. Our calculated LDA barriers are similar to those of Refs. [20–22]. The small discrepancies with Ref. [22] may be due to the different basis sets and to our finer k point sampling. We find that, while the LDA systematically underestimates the interaction energies, it overestimates the barrier heights, relative to the vdW results. Our calculated barriers for the easy direction of armchair and zigzag nanotubes are ~ 3 – 4 times larger than the experimental value of ~ 17 $\mu\text{eV}/\text{atom}$ [17]. Our estimate for the static frictional force, $F_s = (dU/dx)_{\text{max}} = \pi U_G/2\Delta x$, is also larger than the experimental value [18] of 2.3×10^{-14} N/atom by the same factor. Given the experimental uncertainty of the nanotube chiralities, we consider this agreement quite satisfactory.

In conclusion, we have described an efficient $O(N \log N)$ algorithm to include van der Waals interactions through the self-consistent treatment of a nonlocal *ab initio* functional proposed recently [9]. Even for a system of only 50 atoms, the CPU time to calculate the xc potential is $\sim 10^3$ times smaller than with the original $O(N^2)$ formulation [14]. In fact, it is only ~ 10 times larger than with the GGA, i.e., still negligible in any medium or large DFT simulation. Using this implementation, we have calculated the interaction energies, as well as the barriers for relative displacement, between concentric tubes in several armchair, zigzag, and chiral DWNTs.

We would like to thank E. Anglada, E. Artacho, and D. C. Langreth for many discussions and for their help in generating basis sets and testing our implementation, and to J. M. Cela and R. Grima for their help in the parallelization of the code. This work has been funded by Grant No. FIS2006-12117 from the Spanish Ministry of Science.

[1] K. Muller-Dethlefs and P. Hobza, Chem. Rev. **100**, 143 (2000).

- [2] J. M. P. Jorda and A. D. Becke, Chem. Phys. Lett. **233**, 134 (1995).
- [3] S. Tsuzuki and H. P. Luthi, J. Chem. Phys. **114**, 3949 (2001).
- [4] J. F. Dobson, A. White, and A. Rubio, Phys. Rev. Lett. **96**, 073201 (2006).
- [5] M. Elstner, P. Hobza, T. Frauenheim, and E. Kaxiras, J. Chem. Phys. **114**, 5149 (2001).
- [6] S. Grimme, J. Comput. Chem. **25**, 1463 (2004).
- [7] O. A. von Lilienfeld, I. Tavernelli, U. Rothlisberger, and D. Sebastiani, Phys. Rev. Lett. **93**, 153004 (2004).
- [8] J. G. Angyan, I. C. Gerber, A. Savin, and J. Toulouse, Phys. Rev. A **72**, 012510 (2005).
- [9] M. Dion, H. Rydberg, E. Schröder, D. C. Langreth, and B. I. Lundqvist, Phys. Rev. Lett. **92**, 246401 (2004).
- [10] Y. Zhang and W. Yang, Phys. Rev. Lett. **80**, 890 (1998).
- [11] D. C. Langreth, B. I. Lundqvist, S. D. Chakarova-Kack, V. R. Cooper, M. Dion, P. Hyldgaard, A. Kelkkanen, J. Kleis, L. Z. Kong, and S. Li *et al.*, J. Phys. Condens. Matter **21**, 084203 (2009).
- [12] L. C. Balbas, J. L. Martins, and J. M. Soler, Phys. Rev. B **64**, 165110 (2001).
- [13] T. Thonhauser, V. R. Cooper, S. Li, A. Puzder, P. Hyldgaard, and D. C. Langreth, Phys. Rev. B **76**, 125112 (2007).
- [14] The present method has been implemented in a private version of the Abinit plane wave code [X. Gonze *et al.*, Comput. Mater. Sci. **25**, 478 (2002)] and compared with the direct real-space integration method for a variety of systems; D. C. Langreth (private communication).
- [15] L. Kong, G. Roman-Perez, J. M. Soler, and D. C. Langreth, this issue, Phys. Rev. Lett. **103**, 096103 (2009).
- [16] J. Kleis, E. Schröder, and P. Hyldgaard, Phys. Rev. B **77**, 205422 (2008).
- [17] A. Barreiro, R. Rurali, E. Hernandez, J. Moser, T. Pichler, L. Forr, and A. Bachtold, Science **320**, 775 (2008).
- [18] J. Cumings and A. Zettl, Science **289**, 602 (2000).
- [19] R. Saito, R. Matsuo, T. Kimura, G. Dresselhaus, and M. S. Dresselhaus, Chem. Phys. Lett. **348**, 187 (2001).
- [20] E. Bichoutskaia, A. M. Popov, A. El-Barbary, M. I. Heggie, and Y. E. Lozovik, Phys. Rev. B **71**, 113403 (2005).
- [21] J.-C. Charlier and J.-P. Michenaud, Phys. Rev. Lett. **70**, 1858 (1993).
- [22] E. Bichoutskaia, M. I. Heggie, A. M. Popov, and Y. E. Lozovik, Phys. Rev. B **73**, 045435 (2006).
- [23] J. M. Soler, E. Artacho, J. D. Gale, A. García, J. Junquera, P. Ordejón, and D. Sánchez-Portal, J. Phys. Condens. Matter **14**, 2745 (2002).
- [24] P. Ordejón, E. Artacho, and J. M. Soler, Phys. Rev. B **53**, R10441 (1996).
- [25] E. Anglada, J. M. Soler, J. Junquera, and E. Artacho, Phys. Rev. B **66**, 205101 (2002).
- [26] J. Moreno and J. M. Soler, Phys. Rev. B **45**, 13 891 (1992).
- [27] L. X. Benedict, N. G. Chopra, M. L. Cohen, A. Zettl, S. G. Louie, and V. H. Crespi, Chem. Phys. Lett. **286**, 490 (1998).
- [28] See EPAPS Document No. E-PRLTAO-103-047936. For more information on EPAPS, see <http://www.aip.org/pubservs/epaps.html>.
- [29] J. P. Perdew and A. Zunger, Phys. Rev. B **23**, 5048 (1981).
- [30] J. P. Perdew, K. Burke, and M. Ernzerhof, Phys. Rev. Lett. **77**, 3865 (1996).